Observations of low-latitude plasma density enhancements and their associated plasma drifts

J. H. Klenzing,[1] D. E. Rowland,[1] R. F. Pfaff,[1] G. Le,[1] H. Freudenreich,[1] R. A. Haaser,[2] A. G. Burrell,[2] R. A. Stoneback,[2] W. R. Coley,[2] and R. A. Heelis[2]

J. H. Klenzing, NASA Postdoctoral Program Fellow, Space Weather Laboratory, Code 674, Goddard Space Flight Center, Greenbelt, MD 20771, USA. (jeffrey.klenzing@nasa.gov)

[1]Space Weather Laboratory / Code 674,
Goddard Space Flight Center, Greenbelt,
Maryland, USA

[2]Center for Space Sciences, The
University of Texas at Dallas, MS WT15,
Richardson, Texas, USA.

Abstract. Plasma density structures are frequently encountered in the nighttime low-latitude ionosphere by probes on the Communication/Navigation Outage Forecasting System (C/NOFS) satellite. Of particular interest to us here are plasma density enhancements, which are typically observed $\pm 15^{\circ}$ away from the magnetic equator. The low inclination of the C/NOFS satellite offers an unprecedented opportunity to examine these structures and their associated electric fields and plasma velocities, including their field-aligned components, along an east-west trajectory. Among other observations, the data reveal a clear asymmetry in the velocity structure within and around these density enhancements. Previous observations have shown that the peak change in drift velocity associated with a density enhancement occurs simultaneously both perpendicular and parallel to the magnetic field, while the results in this paper show that the peak change in parallel flow typically occurs 25-100 km to the east of the peak perpendicular flow. We discuss this and other aspects of the observations in relation to the characteristics of the plasma depletions formed near the magnetic equator detected by the same probes on the C/NOFS satellite and to previous observations and theories.

1. Introduction

Ionospheric scintillation refers to the scattering of radio waves interacting with an irregular ion density layer in the upper atmosphere and is an important concern for the successful operation of GPS, radar, and other communication signals. For historical reasons, various types of equatorial plasma density irregularities have been classified under the generic name Equatorial Spread-F (ESF) due to their common effect on radar echoes in the F-region Ionosphere [*Kelley*, 2009]. One of the better understood irregularities associated with ESF is the plasma density depletion, also referred to as a plasma "bubble," which is formed by a Rayleigh-Taylor instability acting of the bottomside of the F-layer [*e.g., Fejer and Kelley* 1980]. ESF plasma depletions appear as elongated plumes of relatively low density in radar data [*Woodman and La Hoz*, 1976] and as curved region of reduced optical emission from space-borne imagers [*Kil et al.*, 2009]. More recently, plasma density enhancements, sometimes referred to as "blobs," have been observed in the vicinity in plasma depletions, leading to much discussion about the potential relation between these two density structures.

Plasma enhancements were first reported from ion density and temperature data from the Hinotori satellite [*Oya et al.*, 1986]. They were found to occur beyond the edge of the region of occurrence for bubbles, typically about 15 degrees away from the magnetic equator in either hemisphere. *Watanabe and Oya* [1986] examined the statistics of occurrence and found that enhancements favor the winter hemisphere, typically occur after midnight, and have a strong longitudinal variation pattern that varies as a function of season. Based on a statistical analysis of enhancements and depletions encountered by

Hinotori, they concluded that the two phenomena must have different physical drivers, with the depletions caused by $\mathbf{E}\times\mathbf{B}$ uplift and the enhancements caused by meridional wind instabilities.

However, a number of recent observations have suggested a stronger link between the evolution of bubbles and blobs. Observations from satellites [*Le et al.*, 2003], all-sky imagers [*Pimenta et al.*, 2007; *Martinis et al.*, 2009], radar [*Yokoyama et al.*, 2007], and GPS TEC measurements [*Dashora and Pandey*, 2005] have shown density enhancements forming simultaneously near depletions. *Yokoyama et al.* [2007] shows depletions and enhancements forming along the same flux tube using data from ROCSAT-1 and Equatorial Atmosphere Radar. Density enhancements were also found along the same field lines as ESF airglow depletions [*Martinis et al.*, 2009]. Statistical studies with satellite data from KOMPSAT-1 and DMSP F15 have shown that the depletions and enhancements show similar seasonal and longitudinal variations (with several exceptions) [*Park et al.*, 2008a].

Le et al. [2003] proposes a mechanism to link the two phenomena. Polarization electric fields formed inside the depleted flux tubes are mapped down the magnetic field lines past the region of depletion. These eastward polarization fields result in an upward $\mathbf{E}\times\mathbf{B}$ drift that transports local plasma upward to just above the depleted flux tube, resulting in a plasma density enhancement. This is supported by the similarity of the spectral properties of density fluctuations inside the enhancements and depletions [*Le et al.* 2003] and by the increase in the relative concentration of O^+ to H^+ inside the enhancement [*Yokoyama et al.*, 2007]. Recent simulation work using the SAMI3 model shows that regions of enhanced plasma density can form around spread F depletion plumes [*Krall et al.*, 2010].

The following work discusses recent observations of plasma density enhancements from the C/NOFS satellite and their associated velocity and composition structures during a period of very low solar flux. Both plasma density depletions and enhancements were frequently encountered by the C/NOFS satellite during the first two years of operation [Haaser et al., 2010]. While density enhancements have been observed on a number of satellites including STSAT-1, CHAMP, and KOMPSAT-1 [*Park et al.*, 2003, 2008b], most of these satellites were only capable of measuring density and temperature. With the exception of ROCSAT-1 observations and SAMI3 simulations, there has been little discussion of the ion drifts inside and around the density enhancements. The plasma drifts associated with density enhancements observed by C/NOFS will be compared the drifts associated with density depletions.

2. Measurements

The Communication/Navigation Outage Forecast System (C/NOFS) satellite is part of an Air Force mission to locate, understand, and predict equatorial ionospheric scintillation using satellite measurements, complementary ground-based observations, and physics-based models [*de La Beaujardière et al.*, 2004]. The C/NOFS satellite was launched in April 2008 into a 13° inclination orbit with perigee near 400 km and apogee near 860 km. C/NOFS consists of multiple instrument suites designed to study the ion and neutral populations and their effect on the propagation of communication signals. This study will focus on data from the Vector Electric Field Instrument (VEFI), provided by Goddard Space Flight Center, and the Ion Velocity Meter (IVM), provided by the University of Texas at Dallas.

VEFI consists of multiple sensors, including three electric field double probe booms, a lightning detector, and a 3-axis flux-gate magnetometer [*Pfaff et al.*, 2010]. Of interest to this study are the electric field probes and the magnetometer, which are used to provide the $\mathbf{E}\times\mathbf{B}$ drifts perpendicular to the magnetic field. The two perpendicular directions are defined as the meridional direction (positive outward in the plane of the magnetic meridian) and the zonal direction (positive eastward perpendicular to the meridian plane). The $\mathbf{E}\times\mathbf{B}$ drifts are averaged to one sample per second.

IVM, part of the Coupled Ion-Neutral Dynamics Investigation (CINDI) Mission of Opportunity on C/NOFS, consists of two sub-instruments: the retarding potential analyzer (RPA) and the ion drift meter (IDM). These two instruments provide 3D ion drifts as well as density, composition, and temperature information for the ion population [*Heelis and Hanson*, 1998]. The measured velocities are rotated into the field-aligned reference frame using the VEFI magnetometer measurements, providing the drift component parallel to the magnetic field. The meridional component from the IVM is also compared to that from VEFI. Unfortunately, the drift component from the RPA is not optimized due to the low ion flux during this exceptionally deep solar minimum, so the zonal component from the IVM (as well as the parallel and meridional components where the RPA contribution is significant) will be neglected for the purpose of this study.

The C/NOFS data presented in this paper (Figures 1−6) are arranged into four panels per figure, each containing 5−10 minutes of data. Panel (a) shows the density (N) plotted on a log scale, with the total density plotted in black and the O^+ density plotted in blue. The remainder of the density consists of light ions (H^+ and He^+). Panel (b) shows the parallel drift ($v_{||}$) derived from IVM; it is defined as positive northward. Panel (c) shows

the meridional $\mathbf{E}\times\mathbf{B}$ drift ($v_{\perp m}$) derived from both IVM (green) and VEFI (purple), and panel (d) shows the zonal $\mathbf{E}\times\mathbf{B}$ drift ($v_{\perp z}$) from VEFI. The important features are marked by a vertical orange line that corresponds to the peak change in density as determined by a quadratic fit to the density perturbation. All data is plotted as a function of UT, with the corresponding solar local time (SLT), altitude, magnetic dip angle, and geographic location listed on the x-axis.

3. Observation of Density Depletions

Figures 1 and 2 are examples of plasma density depletions observed by C/NOFS. Note that the depletions shown here are relatively weak (*i.e.*, density is reduced by less than one order of magnitude) compared to other recent studies [*e.g., de La Beaujardière et al.*, 2009] due to the difficulty in calculating accurate three-dimensional ion drifts inside the deep depletions (where density is reduced by several orders of magnitude). These "weak" depletions are similar to the upper regions of a depleted plasma shell as shown in the simulations of *Aveiro and Hysell* [2010]. The two figures show that:

1. The peak change in density occurs nearly simultaneously (*i.e.*, at the same longitude) with the peak change in velocity. This is similar to the ROCSAT observations of plasma depletions in the equatorial ionosphere [*Le et al.*, 2003].

2. A poleward change in drift is associated with most of the observed bubbles. Figure 1 shows several depletions south of the dip equator. The depletions correspond to a negative (southward) change in $v_{||}$. Depletions observed north of the dip equator (Figure 2) have a corresponding postive (norhward) change in $v_{||}$. Depending on the relative strengths of the irregularity and the background drift, the direction of parallel flow may or may not change.

3. The $\mathbf{E}\times\mathbf{B}$ perturbation drifts within the depletions are typically upward (meridional) and westward (zonal), which correspond to a polarization electric field pointing up and east. This corresponds to the fields expected in a westward-tilted plasma bubble [*Huang et al.*, 2010]. There are several events where the zonal drift is noisy, and the relative change associated with the bubble is unclear.

4. Observations of Density Enhancements

Figures 3-6 are examples of density enhancements observed by the C/NOFS satellite, with the associated 3D ion drifts relative to the magnetic field. A vertical line marks a local density increase $\geq$50% above the background density. Plasma density enhancements are observed during solstice and equinox in both magnetic hemispheres. Figures 3-5 show density enhancements near the June solstice of 2009, with orbit tracks in the southern (winter) magnetic hemisphere (Figure 3), in the northern (summer) magnetic hemisphere (Figure 4), and near the magnetic dip equator (Figure 5). Figure 6 shows an event in the southern hemisphere near the September equinox. All four plots show similar features, as outlined below:

1. The enhancements show an increase in relative O^+ concentration, displacing lighter ions. This indicates that plasma is being transported from regions with a lower apex height. This is consistent with previous observations [Yokoyama *et al.*, 2007].

2. A poleward change in ion drift parallel to $\mathbf{B}$ is associated with most of the observed enhancements. Figure 3 shows several examples of enhancements in the southern magnetic hemisphere; Figure 4 shows a series of events in the northern magnetic hemisphere. Note that both events are near the June solstice; consequently, the background parallel drift is

toward the southern (winter) pole. Of the nine events in these two plots, seven show a strong poleward shift in the parallel ion drift associated with the enhancement.

3. The peak change in $\mathbf{E}\times\mathbf{B}$ drift occurs to the west of the peak change in parallel drift. The separation of the peak perturbation drifts ranges from $25-100$ km along the east-west axis. The peak density is typically is found between the two peak drifts. This structure is observed in all seasons and both hemispheres; it is independent of the change in altitude of the orbit track. The apex altitudes associated with the enhancements reported here range from 483 km (Figure 5) to 1045 km (Figure 3). This structure was not reported in previous *in situ* data. *Le et al.* [2003] shows that the peak density occurs at the same longitude as the peak drifts in all three directions for ROCSAT-1 data from 1999-2000.

4. These features are not limited to the higher magnetic latitudes. Figure 5 shows an event with all the characteristics of the density enhancements in the previous two figures, but it occurs near the dip equator. This may be a region of local increased density above a rising depletion as seen in simulation [*Krall et al.*, 2010].

5. Typically, an upward meridional drift and a westward zonal drift are associated with the density enhancements. The perturbations in the $\mathbf{E}\times\mathbf{B}$ drifts are consistent with those seen in the westward-tilted bubbles. A notable exception is the enhancement at 17:05:10 in Figure 6, which shows a strong eastward drift in panel (d). The perturbation drifts inside this enhancement are similar to those observed inside an eastward-tilted bubble[*Huang et al.*, 2010]. Note that both the "eastward-tilted" and "westward-tilted" enhancements observed in Figure 6 show the same longitudinal offset between the perpendicular and parallel drifts.

5. Discussion

While the low inclination of the C/NOFS orbit restricts the longitudinal coverage of the satellite at the magnetic latitudes where density enhancements are typically expected, density enhancements are frequently encountered by C/NOFS. This is consistent with the statistical studies by *Park et al.* [2008a], which show that the average magnetic latitude where enhancements are found decreases as solar activity decreases. The following discussion is not meant to be an exhaustive study of the qualities of density enhancements during extreme solar minimum; instead it provides additional insight into the structure of density enhancements not previously discussed in the published literature.

5.1. Comparison to previous observations

The observations from C/NOFS show a number of similarities to previous observations, but are markedly different in the velocity structure across the plasma density enhancement. As stated in the previous section, the peak change in ion drift parallel to the magnetic field occurs 25−100 km to the east of the peak change in the drift perpendicular to **B**. To better compare these events to previous *in situ* studies of plasma density enhancements, several of the plasma enhancements observed in data from ROCSAT-1 are plotted in Figure 7. These particular events are discussed in greater detail in *Le et al.* [2003]. The perturbation drifts associated with the enhancement all peak simultaneously (*i.e.*, at the same longitude) for the events observed by ROCSAT.

It should be noted that ROCSAT has a larger orbital inclination than C/NOFS (35° as compared to 13°). Consequently, the typical orbit of C/NOFS is nearly perpendicular to the geomagnetic field lines, while the angle between a typical ROCSAT orbit and **B** is smaller (∼50° in the case of Figure 7). Despite these differences, it is not expected that

193 the ROCSAT orbit track relative to the flux tube containing the density structures would
194 mask a separation between the velocity peaks as observed in the C/NOFS data.

195 A potential source of the difference between the C/NOFS and ROCSAT observations
196 is solar activity. The C/NOFS satellite has the distinction of being launched during the
197 deepest solar minimum to occur since the dawn of the space age. The C/NOFS events
198 shown here were measured when F10.7 was less than 70 sfu, while the ROCSAT event
199 was measured when F10.7=147.9. Additionally, during 2008 the H^+/O^+ transition height
200 was significantly lower than predicted by the IRI model for an accurate input of F10.7,
201 indicating that the ionosphere is contracted further than expected [*Heelis et al.*, 2009].
202 Evidence of a "contracted" ionosphere is supported by the comparison between the unper-
203 turbed regions around the enhancements in Figures 3-6 and those from ROCSAT. Despite
204 the fact that the ROCSAT observations are 200 km higher in altitude, they are associ-
205 ated with ion densities nearly an order of magnitude greater than those observed with
206 C/NOFS. Figure 7 also shows a greater relative concentration of O^+ in the unperturbed
207 background than the previous figures.

5.2. Relation between depletions and enhancements

208 The perturbation $\mathbf{E}\times\mathbf{B}$ drifts observed inside the enhancements are similar to those
209 observed in the depletions. Both types of density irregularities typically are associated
210 with an upward change in meridional drift and a westward change in the zonal drift. This
211 is consistent with previous studies that suggest that polarization electric fields within a
212 density depletion are mapped down the geomagnetic field lines, forming a density en-
213 hancement above the depleted flux tube. There is a longitudinal offset between the peak
214 parallel and $\mathbf{E}\times\mathbf{B}$ drifts in the density enhancements, while the ion drifts peak in all three

directions at or near the same longitude for the depletions. The existence of a longitudinal offset is persistent in the observations and independent of changes in the orbit track relative to the flux tube.

Simulations using the SAMI3 model have shown that a slowly growing ESF plume can produce $\mathbf{E}\times\mathbf{B}$ drifts that lift density upward faster than gravity moves it downward [*Krall et al.*, 2010]. This effect occurs in simulations for low solar activity (F10.7 <100) or when the growth of a plume is slowed by a mild trans-hemispheric wind. The slow growth leads to a weak super fountain [*Huba et al.*, 2009a] with perturbation drifts inside the irregularities on the order of 200 m/s. This is very similar to the C/NOFS observations, but the simulations do not show the longitudinal offset between the peak parallel and perpendicular drift velocities [*Krall et al.*, 2009, 2010]. The lack of this offset may be due in part to unique conditions during the recent extreme solar minimum.

The presence of a longitudinal offset may also indicate that the physics relating depletions and enhancements must be better understood in three spatial dimensions. Instead of looking merely at a depleted flux tube, a three-dimensional structure is needed to explain the asymmetric velocity structure around the density enhancement. The depletion shell model described in *Kil et al.* [2009] would provide the necessary longitudinal asymmetry. Alternatively, zonal wind effects may also produce the necessary structure [*Huba et al.*, 2009b].

6. Summary and Future Work

The ion drift velocities inside and around plasma density enhancements observed by C/NOFS are found to have a more complicated structure than previously reported. The perturbation $\mathbf{E}\times\mathbf{B}$ drifts associated with the enhancements are similar to those observed

within plasma depletions. However, the longitudinal separation between the peak $\mathbf{E}\times\mathbf{B}$ and parallel drifts is a feature previously unreported either in data or in models. It is unclear whether the longitudinal offset is unique to the recent protracted solar minimum or if it is a relatively common feature that has yet to be observed due to the sparse coverage of *in situ* measurements of three-dimensional drifts within plasma density enhancements. This uncertainty is likely to be resolved as the C/NOFS satellite continues to take data during the transition back to solar maximum over the next few years.

The plasma density enhancements in this paper were chosen to represent general observations in the C/NOFS data set. A statistical study of the plasma irregularities observed by C/NOFS and the relation of three-dimensional ion drifts within these features is in progress. Further discussion of the three-dimensional nature of plasma depletion shells and associated enhancements is needed to relate these new observations to current theory.

Acknowledgments. JHK is supported by an appointment to the NASA Postdoctoral Program at Goddard Space Flight Center, administered by Oak Ridge Associated Universities through a contract with NASA. The authors would like to thank C. S. Huang for helpful discussions regarding the electric field structure inside and around plasma density depletions. The Communication/Navigation Outage Forecast System (C/NOFS) mission, conceived and developed by the Air Force Research Laboratory, is sponsored and executed by the USAF Space Test Program.

References

Aveiro, H. C., and D. L. Hysell, (2010), "Three-dimensional numerical simulation of equatorial F region plasma irregularities with bottomside shear flow," *J. Geophys. Res.,*

115, A11321, doi:10.1029/2010JA015602.

Dashora, N., and R. Pandey (2005), "Observations in equatorial anomaly region of total electron content enhancements and depletions," *Ann. Geophys., 23,* 2449-2456.

de La Beaujardière, O., and the C/NOFS Definition Team (2004), "C/NOFS: a mission to forecast scintillations," *J. Atmos. and Sol-Terr. Phys,, 66,* 1573, doi:10.1016/j.jastp.2004.07.030.

de La Beaujardière, O., J. M. Retterer, R. F. Pfaff, P. A. Roddy, C. Roth, W. J. Burke, Y. J. Su, M. C. Kelley, R. R. Ilma, G. R. Wilson, L. C. Gentile, D. E. Hunton, and D. L. Cooke (2009), "C/NOFS observations of deep plasma depletions at dawn," *Geophys. Rev. Lett., 36,* L00C06, doi:10.1029/2009GL038884.

Fejer, B. G., and M. C. Kelley (1980), "Ionospheric Irregularities," *Rev. Geophys. Space Phys., 18*, 401.

Haaser, R. A., G. D. Earle, R. A. Heelis, J. H. Klenzing, W. R. Coley, R. A. Stoneback, A. G. Burrell (2010), "A study of ionospheric low latitude velocity and density irregularity correlations during solar minimum," Abstract SA51B-1624 presented at 2010 Fall Meeting, AGU, San Francisco, Calif., 13-17 Dec.

Heelis, R. A., and W. B. Hanson, "Measurements of thermal ion drift velocity and temperature using planar sensors," in *Measurement Techniques in Space Plasmas (Geophys. Monogr. Ser. vol. 102)*, edited by R. F. Pfaff, J. E. Borovsky, and D. T. Young, (AGU, Washington, D. C., 1998) p. 61

Heelis, R. A., W. R. Coley, A. G. Burrell, M. R. Hairston, G. D. Earle, M. D. Perdue, R. A. Power, L. L. Harmon, B. J. Holt, and C. R. Lippincott (2009), "Behavior of the O+/H+ transition height during the extreme solar minimum of 2008," *Geophys. Res.*

Lett., 36, L00C03, doi:10.1029/2009GL038652.

Huang, C.-S., O. de La Beaujardière, R. F. Pfaff, J. M. Retterer, P. A. Roddy, D. E. Hunton, Y.-J. Su, S.-Y. Su, and F. J. Rich (2010), "Zonal drift of plasma particles inside equatorial plasma bubbles and its relation to the zonal drift of the bubble structure," *J. Geophys. Res., 115* A07316, doi:10.1029/2010JA015324.

Huba, J. D., J. Krall, and G. Joyce (2009a), "Atomic and molecular ion dynamics during equatorial spread F," *Geophys. Rev. Lett., 36,* L10106, doi:10.1029/2009GL037675.

Huba, J. D., S. L. Ossakaw, G. Joyce, J. Krall, and S. L. England (2009b), "Three-simensional equatorial spread F modeling: Zonal neutral wind effects," *Geophys. Rev. Lett., 36,* L19106, doi:10.1029/2009GL040284.

Kelley, M. C. (2009), "The Earth's Ionosphere: Plasma Physics and Electrodynamics," Academic Press, Burlington, MA, 2^{nd} edition,

Kil, H., R. A. Heelis, L. J. Paxton, and S.-J. Oh (2009), "Formation of a plasma depletion shell in the equatorial ionosphere," *J. Geophys. Res., 114,* A11302 doi:10.1029/2009JA014369.

Krall, J., J. D. Huba, and C. R. Martinis (2009), "Three-dimensional modeling of equatorial spread F airglow measurements," *Geophys. Rev. Lett., 36,* L10103, doi:10.1029/2009GL038441.

Krall, J., J. D. Huba, G. Joyce, and T. Yokoyama (2010), "Density enhancements associated with equatorial spread F," *Ann. Geophys., 28,* 327-337, www.ann-geophys.net/28/327/2010/.

Le, G., C.-S. Huang, R. F. Pfaff, S.-Y. Su, H.-C. Yeh, R. A. Heelis, F. J. Rich, and M. Hairston (2003), "Plasma density enhancements associated with equato-

rial spread F: ROCSAT-1 and DMSP observations," *J. Geophys. Res., 108,* 1318, doi:10.1029/2002JA009592.

Martinis, C., J. Baumgardner, M. Mendillo, S.-Y. Su, and N. Aponte (2009), "Brightening of 630.0 nm equatorial spread-F airglow depletions," *J. Geophys. Res., 114,* A06318, doi:10.1029/2008JA013931.

Oya, H., T. Takahashi, adn S. Watanabe (1986), "Observations of Low Latitude Ionosphere by the Impedance Probe on Board the Hinotori Satellite," *J. Geomag. Geoelectr., 38,* 111-123

Park, J., K. W. Min, J.-J. Lee, H. Kil, V. P. Kim, H.-J. Kim, E. Lee, and D. Y. Lee (2003), "Plasma blob events observed by KOMPSAT-1 and DMSP F15 in the low latitude nighttime upper ionosphere," *Geophys. Res. Lett., 30*, 2114, doi:10.1029/2003GL018249.

Park, J., K. W. Min, V. P. Kim, H. Kil, H. J. Kim, J. J. Lee, E. Lee, S. J. Kim, D. Y. Lee, M. Hairston (2008), "Statistical description of low-latitude plasma blobs as observed by DMSP F15 and KOMPSAT-1," *Adv. Space Res., 41,* 650-654, doi:10.1016/j.asr.2007.04.089.

Park, J., K. W. Min, V. P. Kim, H. Kil, H. J. Kim, J. J. Lee, E. Lee, S. J. Kim, D. Y. Lee, M. Hairston (2008), "Magnetic signatures and conjugate features of low-latitude plasma blobs as observed by the CHAMP satellite," *J. Geophys. Res., 113,* A09313 doi:10.1016/j.asr.2008Ja013211.

Pfaff, R., D. Rowland, H. Freudenreich, K. Bromund, G. Le, M. Acuña, J. Klenzing, C. Liebrecht, S. Martin, W. J. Burke, N. C. Maynard, D. E. Hunton, P. A. Roddy, J. O. Ballenthin, and G. R. Wilson (2010), "Observations of DC Electric Fields in the Low Latitude Ionosphere and Their Variations with Local Time, Longitude, and

Plasma Density during Extreme Solar Minimum," *J. Geophys. Res., 115,* A12324, dio:10.1029/2010JA016023.

Pimenta, A., Y. Sahai, J. A. Bittencourt, and F. J. Rich (2007), "Ionospheric plasma blobs observed by OI 630 nm all-sky imaging in the Brazilian tropical sector during the major geomagnetic storm of April 6-7, 2000," *Geophys. Rev. Lett., 34,* L02820, doi:10.1029/2006GL028529.

Watanabe, S., and H. Oya (1986), "Occurrence Characteristics of Low Latitude Ionosphere Irregularities Observed by Impedance Probe on Board the Hinotori Satellite," *J. Geomag. Geoelectr., 38,* 125-149.

Woodman, R. F., and C. La Hoz (1976), "Radar Observations of F Region Equatorial Irregularities," *J. Geophys. Res., 81,* p 5447.

Yokoyama, T., S.-Y. Su, and S. Fukao (2007), "Plasma blobs and irregularities concurrently observed by ROCSAT-1 and Equatorial Atmosphere Radar," *J. Geophys. Res., 112,* A05311, doi:10.1029/2006JA012044.

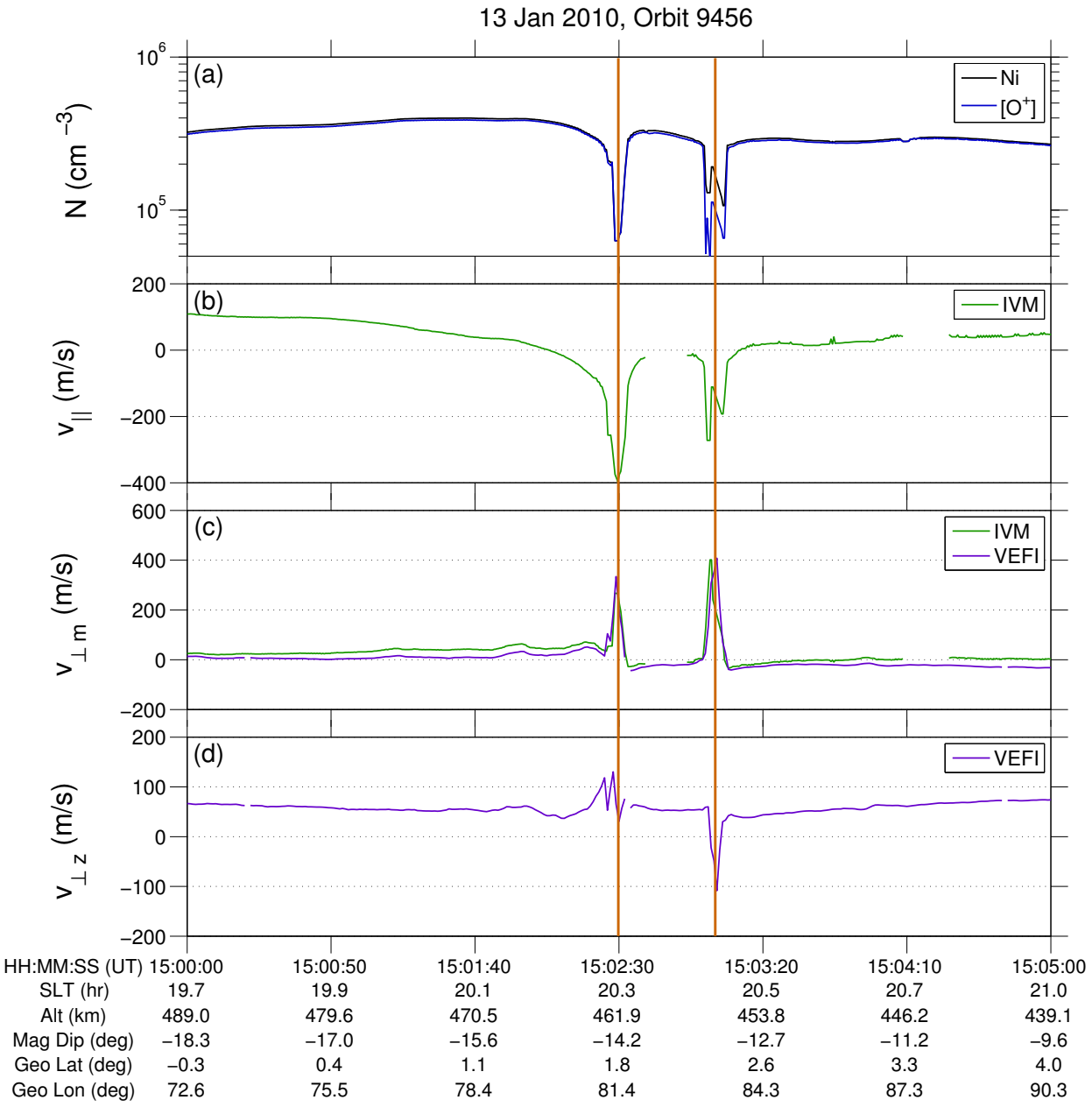

Figure 1. Plasma density depletions observed south of the magnetic dipole equator. The panels show (a) total ion density (along with the O^+ density; the remainder is H^+ and He^+), (b) ion drift parallel to the magnetic field (positive northward), (c) $\mathbf{E}\times\mathbf{B}$ meridional drift (positive upward), and (d) $\mathbf{E}\times\mathbf{B}$ zonal drift (positive eastward). The three events exhibit a clear poleward (negative) change in the parallel drift. The apex altitude for these events is 567 km.

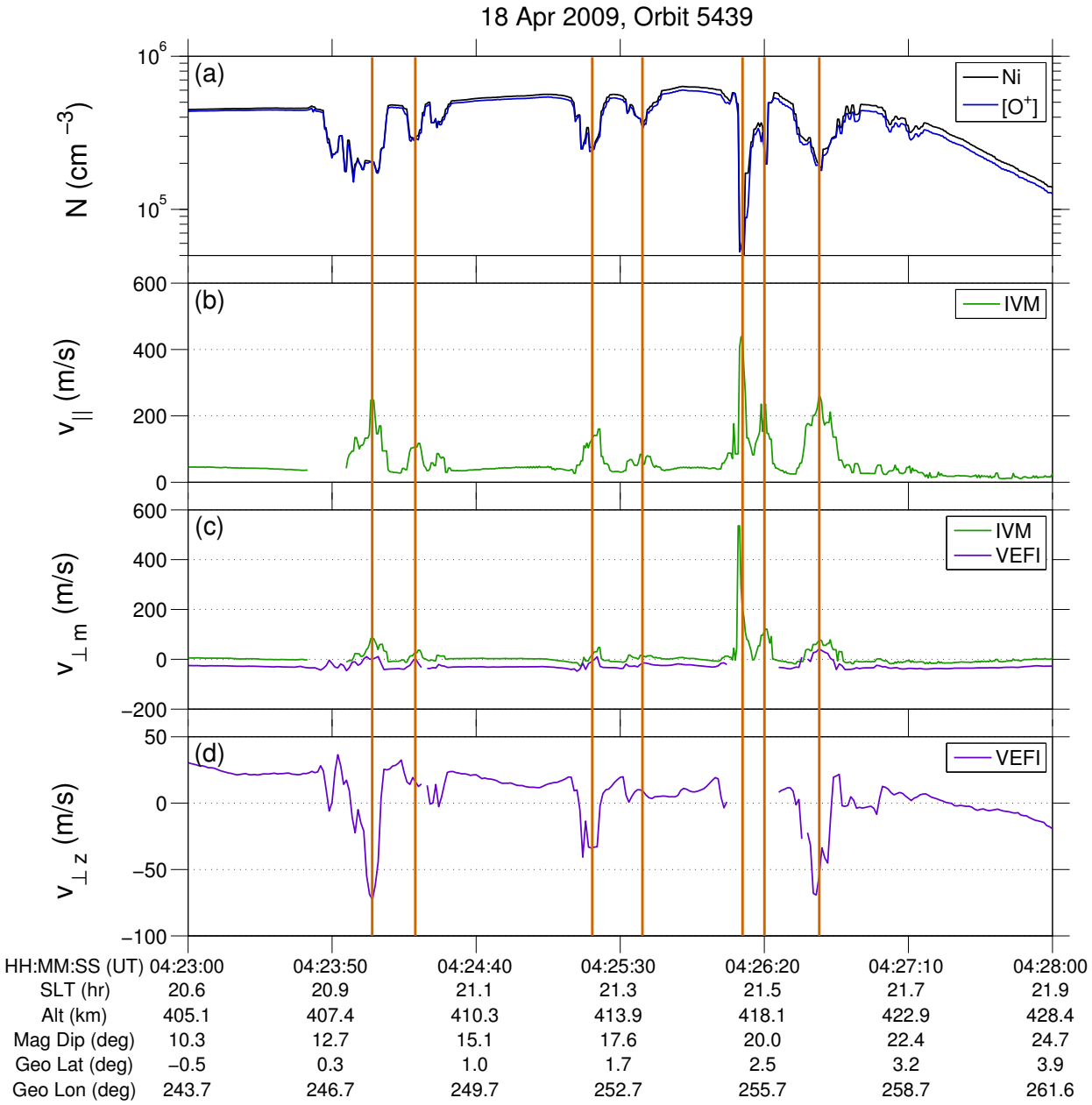

Figure 2. Plasma density depletions observed north of the magnetic dipole equator. All events exhibit a clear poleward (positive) change in the parallel drift. The format is the same as in Figure 1. The apex altitude for these events is 596 km.

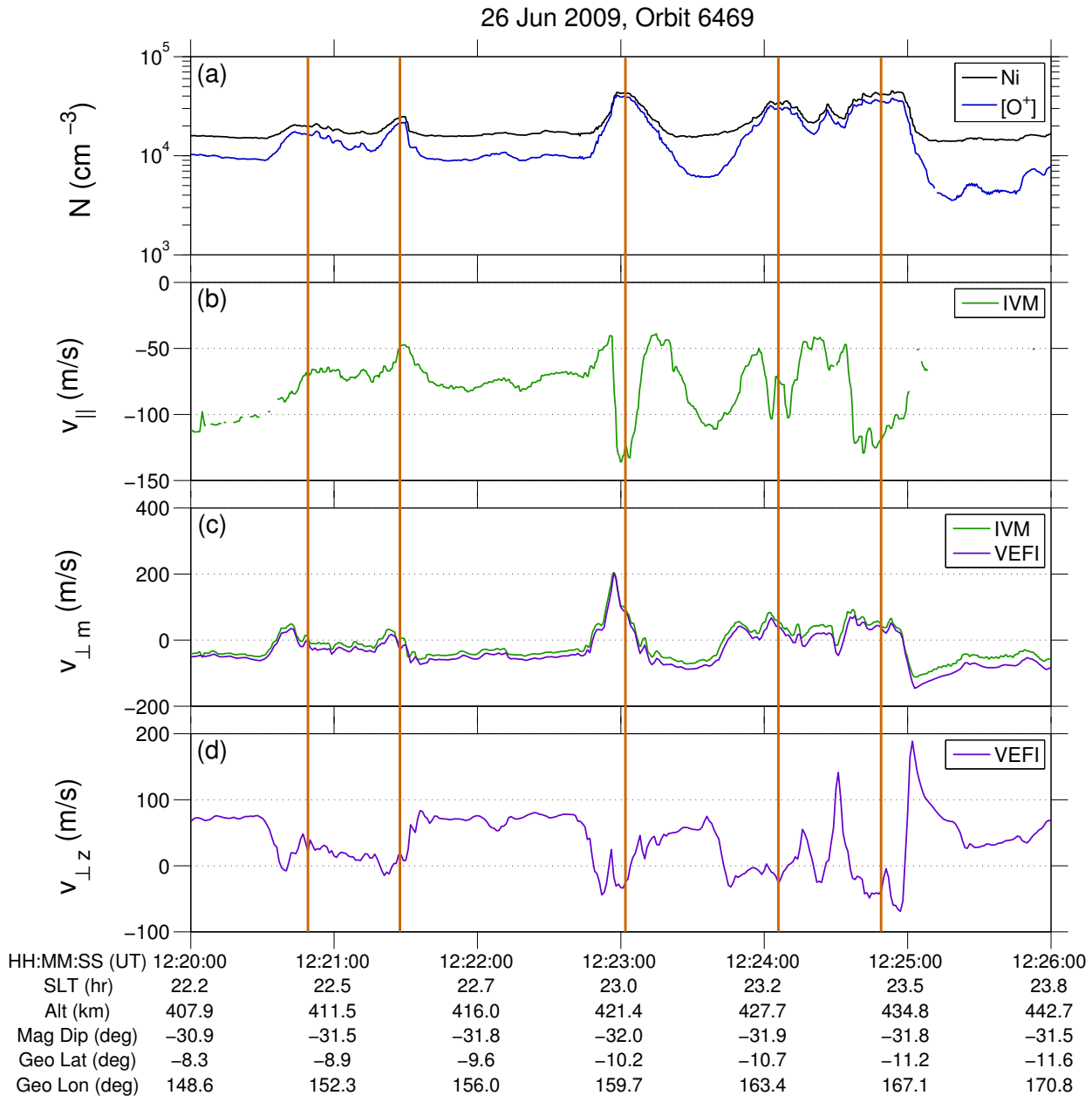

Figure 3. Plasma density enhancements observed near June Solstice 2009 in the southern magnetic hemisphere. Two of the events exhibit a clear poleward (negative) change in the parallel drift, while the two weakest density enhancements show an equatorward (positive) drift. The apex altitude for these events is 1045 km.

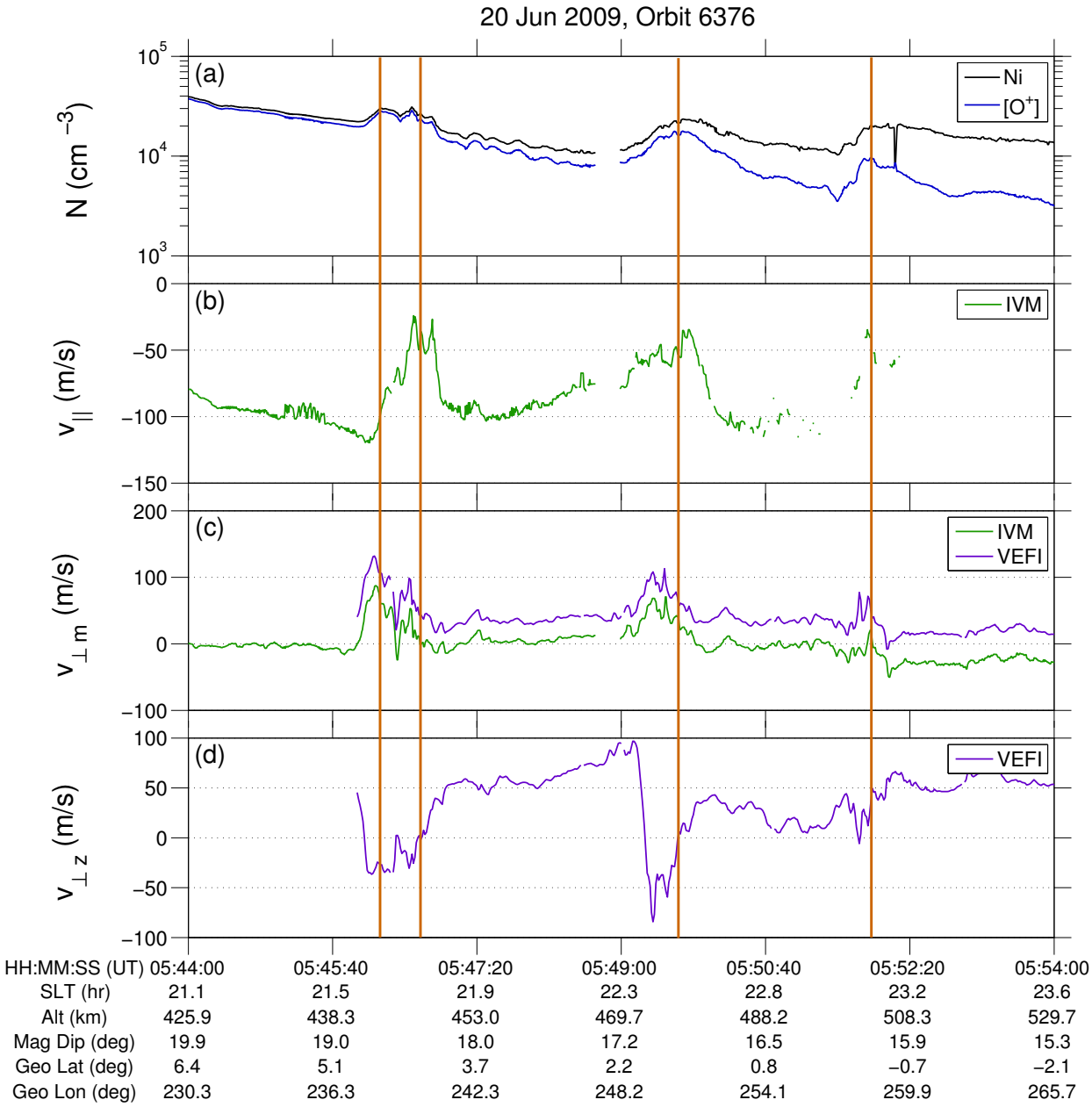

Figure 4. Plasma density enhancements observed near June solstice 2009 in the northern magnetic hemisphere. All of the events show a poleward (positive) change in parallel flow. The apex altitude for these events is 636 km.

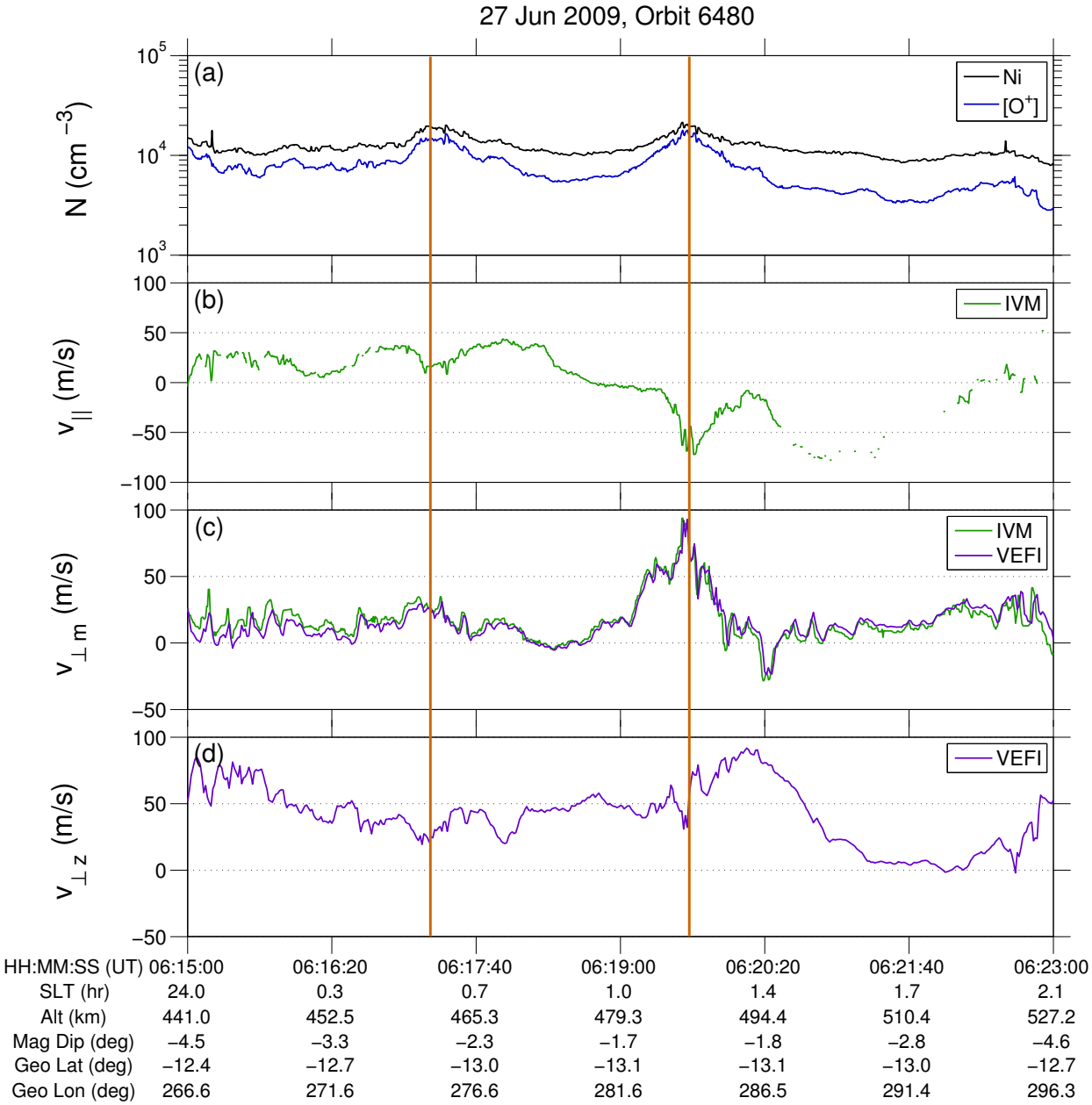

Figure 5. Plasma density enhancements observed near June Solstice 2009 near the magnetic equator. The apex altitude for these events is 483 km.

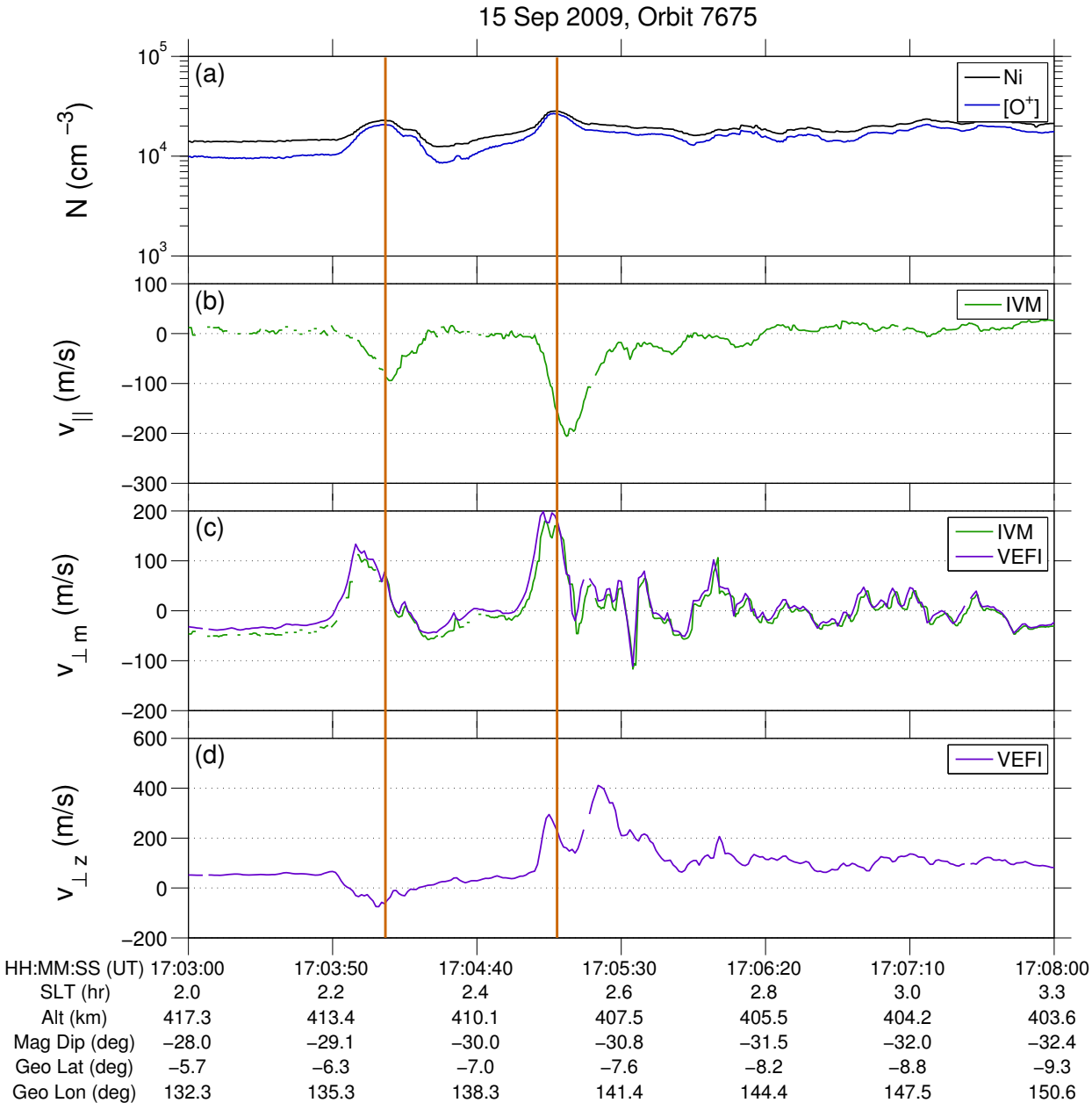

Figure 6. Plasma density enhancements observed near September Equinox 2009 in the southern magnetic hemisphere. The enhancement near 17:05:10 is associated with eastward perturbation drift. The apex altitude for these events is 974 km.

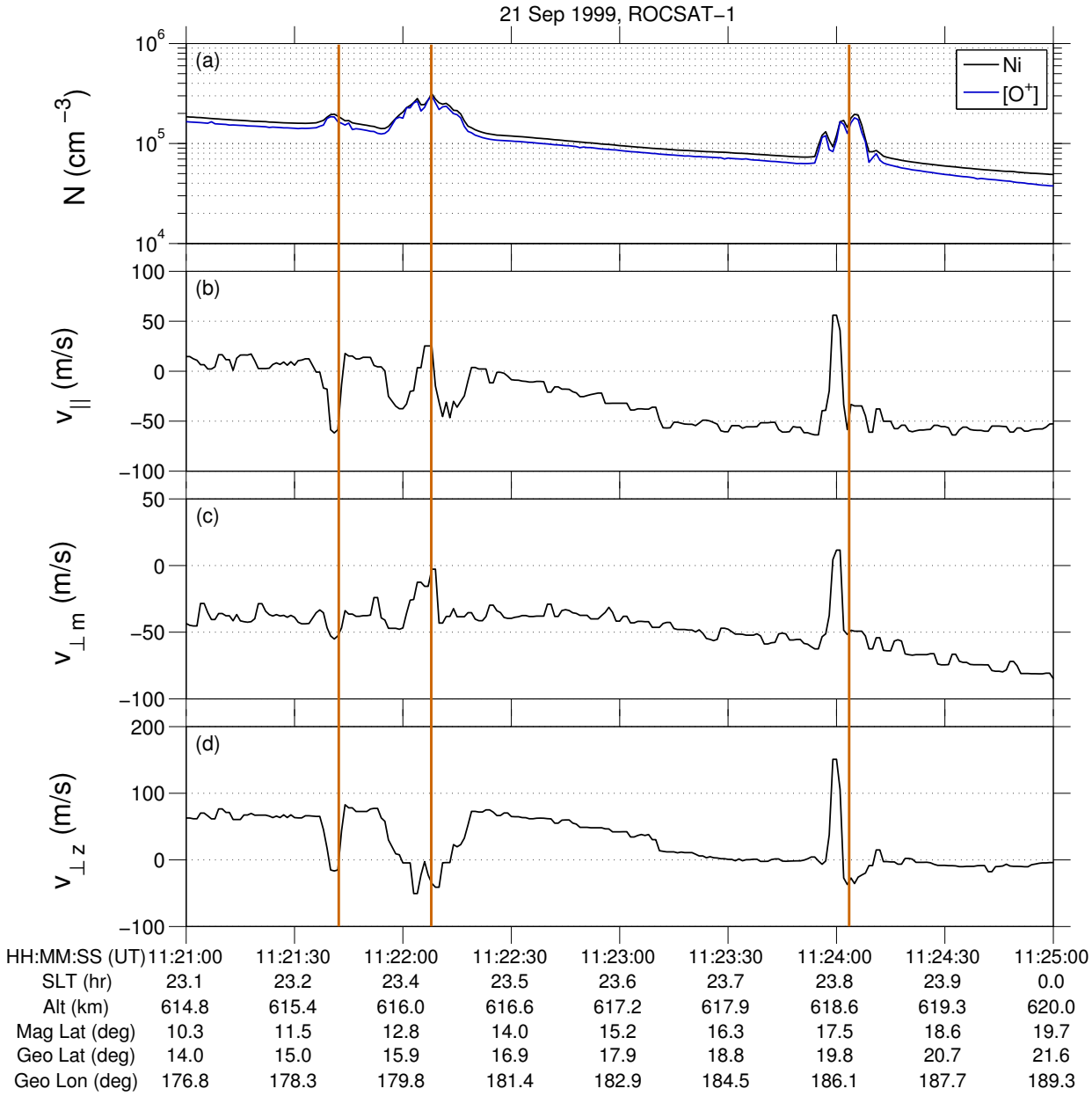

Figure 7. Plasma density enhancements observed from the ROCSAT-1 satellite. These events are discussed in detail in Le *et al.* [2003].